


Article

Research on Dynamic Modeling of KF Algorithm for Detecting Distorted AC Signal

Haoyao Nie ^{1,2} and Xiaohua Nie ^{3,*} 

¹ School of Economics and Management, Nanchang University, Nanchang 330031, China; hynie003@outlook.com

² I.H. Asper School of Business, University of Manitoba, Winnipeg, MB R3T 5V4, Canada

³ Department of Energy and Electrical Engineering, Nanchang University, Nanchang 330031, China

* Correspondence: niexiaoh@163.com

Abstract: Kalman filter (KF) is often based on two models, which are phase angle vector (PAV) model and orthogonal vector (OV) model, in the application of distorted grid AC signal detection. However, these two models lack rigorous and detailed derivation from the principle of dynamic modeling. This paper presents a phase angle vector dynamic (PAVD) model and an orthogonal vector dynamic (OVD) model, which are combined with Kalman filter for detecting distorted grid AC signal. They reveal that the state noise covariance of the dynamic model–based KF is related to the sampling cycle, and overcome the defect of more detecting error for conventional model–based KF. Experiment and evaluation results show that the proposed KF algorithms are reasonable and effective. Therefore, this paper contributes a guiding significance for the application of KF algorithm in harmonic detection.

Keywords: distorted AC signal; Kalman filter; phase angle dynamic model; orthogonal vector dynamic model; state noise covariance; sampling cycle



Citation: Nie, H.; Nie, X. Research on Dynamic Modeling of KF Algorithm for Detecting Distorted AC Signal. *Energies* **2021**, *14*, 8175. <https://doi.org/10.3390/en14238175>

Academic Editor: Jaroslaw Krzywanski

Received: 5 November 2021
Accepted: 2 December 2021
Published: 6 December 2021

Publisher's Note: MDPI stays neutral with regard to jurisdictional claims in published maps and institutional affiliations.



Copyright: © 2021 by the authors. Licensee MDPI, Basel, Switzerland. This article is an open access article distributed under the terms and conditions of the Creative Commons Attribution (CC BY) license (<https://creativecommons.org/licenses/by/4.0/>).

1. Introduction

The Kalman filter (KF) plays an increasingly important role in the real–time detection of grid AC signal [1]. It was first applied to the power signal processing field by Dr. A. A. Girgis in 1981 [2–4]. It mainly applies to the following fields: fundamental and harmonic components detection of grid voltage/current [5–10], phase–locked loop synchronization [11–15], power quality detection and compensation equipment [16–20], power disturbance feature extraction and machine classification [21–24], and etc. In these applications, two conventional models, phase angle vector (PAV) model and orthogonal vector (OV) model, are mainly used. The phase angles were used as vectors to establish a state-space model which could be called the phase angle vector (PAV) model through cosine expansion [3]. The orthogonal vector was used to establish a state-space model that could be called the orthogonal vector (OV) model [4]. However, the state noise covariance of the two models is only a given value based on empirical statistics of the AC signal. It is selected as a fixed value, such as $Q = 0.05 \times I$ (I represents the unit matrix), when AC signal is the grid voltage [10,11]. It is selected as a fixed value, such as $Q = 0.01 \times I$, when the AC signal is the sampling current [20]. It is mainly to avoid big tracking error and enable to detect response without time delay. With the development of computer hardware and sensor technology, the sampling cycle is getting smaller, and the accuracy requirements are getting higher. The detecting accuracy of the fundamental and harmonics components for the conventional detecting model–based KF algorithm cannot meet the requirements of modern engineering applications.

The current issue is that the detecting accuracy of the fundamental and harmonics components for the conventional detecting model–based KF algorithm cannot meet the requirements of modern engineering applications. There is no fixed rule as references

to find the fixed value by applying different sampling cycles. As a result, the detection accuracy cannot achieve the expected goal.

Also, the discretization model lacks of theoretical basis. In view of the fact that the previous literature did not detailedly derive the PAV and OV model from the principle of dynamic modeling. This paper proposes a phase angle vector dynamic (PAVD) model-based KF (PAVD-KF) algorithm and the orthogonal vector dynamic (OVD) model-based KF algorithm (OVD-KF) through model derivation according to the stochastic process theory [12]. It reveals that the state noise covariance of the conventional detecting model is related to the sampling cycle.

This paper contributes:

- (1) We derive the discretization model from the continuous differential equation in accordance with stochastic process theory, to find the value law of fixed value of covariance under different sampling cycles.
- (2) We greatly improve the detecting accuracy of fundamental and harmonics components, enabling the detection results to meet the requirements of modern engineering applications of AC current and voltage signal.

Section 1 introduces the Kalman filter mainly applies to the following fields and model-based KF existing problems. In Section 2, the related works about conventional PAV and OV model are introduced. In Section 3, the PAVD and OVD models are rederived according to of stochastic process theory. Then, the PAVD-KF and OVD-KF algorithms are proposed. In Section 4, the performances of PAVD-KF and OVD-KF algorithms are evaluated and compared by the experimental current and voltage sampling data. Section 5 concludes the paper.

2. Related Work

In this section, we proposed the expression of distorted AC signal first, and introduce the conventional PAV-KF and OV-KF algorithms then.

2.1. Distorted AC Signal

The waveform of the distorted AC signals sampled at time t can be expressed as

$$s(t) = \sum_{i=1}^N A_i(t) \sin[i\omega_0 T + \theta_i(t)] + \sum_{i=1}^N w_i(t) \quad (1)$$

where $i = 1, 2, 3, \dots, N$, T denotes the sampling cycle. For the fundamental frequency of 50 Hz, $\omega_0 = 100\pi$. $\sum_{i=1}^N A_i(t) \sin[i\omega_0 T + \theta_i(t)]$ represents the fundamental and harmonic components. $\sum_{i=1}^N w_i(t)$ is the state noise of fundamental and harmonic components.

2.2. PAV Model

The vector of fundamental and harmonic components is expressed as

$X_k = [x_1 \ y_1 \ \dots \ x_n \ y_n]^T$, where $x_1 = A_1 \cos \theta_1$, $y_1 = A_1 \sin \theta_1$, $x_n = A_n \cos \theta_n$, $y_n = A_n \sin \theta_n$.

The measurement equation of model is expressed as [3]

$$z_k = H_k X_k + V_k = \begin{bmatrix} \cos(\omega_0 kT) \\ -\sin(\omega_0 kT) \\ \vdots \\ \cos(n\omega_0 kT) \\ -\sin(n\omega_0 kT) \end{bmatrix}^T \begin{bmatrix} x_1 \\ y_1 \\ \vdots \\ x_n \\ y_n \end{bmatrix}_k + V_k \quad (2)$$

The state equation of model is expressed as

$$X_{k+1} = \Phi_k X_k + W_k = \begin{bmatrix} 1 & 0 & \cdots & 0 & 0 \\ 0 & 1 & \cdots & 0 & 0 \\ \vdots & \vdots & \ddots & \vdots & \vdots \\ 0 & 0 & \cdots & 1 & 0 \\ 0 & 0 & \cdots & 0 & 1 \end{bmatrix} \begin{bmatrix} x_1 \\ y_1 \\ \vdots \\ x_n \\ y_n \end{bmatrix}_k + \begin{bmatrix} W_{x_1} \\ W_{y_1} \\ \vdots \\ W_{x_n} \\ W_{y_n} \end{bmatrix}_k \quad (3)$$

The covariance matrix of state noise W_k can be expressed as

$$Q_k = E[W_k W_k^T] = \sigma_{PAV}^2 I_{2n \times 2n} \quad (4)$$

2.3. OV Model

Considering a signal $A_k \sin(\omega_k t_k + \theta_k)$ with amplitude A_k , angular frequency is ω_k and phase is θ_k [4,11]. Let $x_k = A_k \sin(\omega_k t_k + \theta_k)$, $y_k = A_k \cos(\omega_k t_k + \theta_k)$, initially, consider $A_{k+1/k} \approx A_k$, $\omega_{k+1/k} \approx \omega_k$ and $\theta_{k+1/k} \approx \theta_k$. At the time $t_{k+1} = t_k + T$, the signal x_k can be expressed as

$$x_{k+1} = A_{k+1} \sin(\omega_k t_k + \omega_k T + \theta_k) = x_k \cos(\omega_k T) + y_k \sin(\omega_k T) \quad (5)$$

where, T is the sampling cycle. Additionally,

$$y_{k+1} = A_{k+1} \cos(\omega_k t_k + \omega_k T + \theta_k) = -x_k \sin(\omega_k T) + y_k \cos(\omega_k T) \quad (6)$$

the state–space is extended for detection of distorted AC signal existed n frequencies harmonic components.

The vectors are expressed as $X_k = [x_1 \ y_1 \ \cdots \ x_n \ y_n]^T$, where, $x_{1k} = A_{1k} \sin(\omega_k t_k + \theta_{1k})$, $y_{1k} = A_{1k} \cos(\omega_k t_k + \theta_{1k})$, $x_{nk} = A_{nk} \sin(n\omega_k t_k + \theta_{nk})$, $y_{nk} = A_{nk} \cos(n\omega_k t_k + \theta_{nk})$.

Then, the state and measurement equation is expressed as [4]

$$\begin{cases} X_{k+1} = \begin{bmatrix} \Phi_1 & \cdots & 0 \\ \vdots & \ddots & \vdots \\ 0 & \cdots & \Phi_n \end{bmatrix} X_k + W_{i_k} \\ z_k = [1 \ 0 \ \cdots \ 1 \ 0] X_k + V_k \end{cases} \quad (7)$$

where, the state transition matrixes Φ_i are shown below as

$$\Phi_i = \begin{bmatrix} \cos(i\omega_k T) & \sin(i\omega_k T) \\ -\sin(i\omega_k T) & \cos(i\omega_k T) \end{bmatrix} \quad (8)$$

The covariance matrix of state noise W_{k_i} can be expressed as

$$Q_{i_k} = E[W_{i_k} W_{i_k}^T] = \sigma_{OV}^2 I_{2n \times 2n} \quad (9)$$

in (4) and (9), $I_{2n \times 2n}$ is a unit matrix. σ_{PAV}^2 and σ_{OV}^2 are selected as 0.05, when AC signal is sampling voltage [10,11]. σ_{PAV}^2 and σ_{OV}^2 are selected as 0.01, when AC signal is sampling current [20].

2.4. PAV-KF and OV-KF Algorithm

The discrete PAV–KF and OV–KF algorithm for detecting distorted AC signal can be expressed as follow by combining PAV and OV model.

$$\begin{cases} \hat{X}_{k+1/k+1} = \Phi_k \hat{X}_{k+1/k} + K_{k+1} (Z_{k+1} - H_k \hat{X}_{k+1/k}) \\ K_{k+1} = \Phi_k P_{k+1/k} H_k^T (H_k P_{k+1/k} H_k^T + R_k)^{-1} \\ P_{k+1/k+1} = \Phi_k P_{k+1/k} \Phi_k^T - K_{k+1} H_k P_{k+1/k} \Phi_k^T + Q_k \end{cases} \quad (10)$$

The amplitude and the phase angle for the fundamental and harmonic components can be calculated as follows.

$$A_{i_{k+1}} = \sqrt{\hat{x}_{i_{k+1}}^2 + \hat{y}_{i_{k+1}}^2} \quad (11)$$

$$\phi_{i_{k+1}} = \arctan\left(\frac{\hat{x}_{i_{k+1}}}{\hat{y}_{i_{k+1}}}\right) \quad (12)$$

3. PAVD-KF and OVD-KF Algorithm

In Section 3, we construct the AC signal continuous differential equation of phase angle vector and orthogonal vector, and derive the discretization PAVD and OVD model in accordance with stochastic process theory. Next, we combine the proposed models with KF algorithm, to obtain PAVD–KF and OVD–KF algorithm.

3.1. PAVFIGURE

D-KF Algorithm

The phase angle vectors of fundamental components in (2)–(3) are expressed as

$$\begin{cases} x(t) = A \cos \theta \\ y(t) = A \sin \theta \end{cases} \quad (13)$$

The first derivative can be expressed as

$$\frac{d}{dt} \begin{bmatrix} x(t) \\ y(t) \end{bmatrix} = A \begin{bmatrix} x(t) \\ y(t) \end{bmatrix} + B \begin{bmatrix} w_x(t) \\ w_y(t) \end{bmatrix} \quad (14)$$

where, $w_x(t)$ and $w_y(t)$ are the input white noise, $w_x(t) \perp w_y(t)$. $w_x(t) \sim (0, \sigma_w^2)$, $w_y(t) \sim (0, \sigma_w^2)$. Where, $A = \begin{bmatrix} 0 & 0 \\ 0 & 0 \end{bmatrix}$, $B = \begin{bmatrix} 1 & 0 \\ 0 & 1 \end{bmatrix}$.

Equation (11) is discretized, and the state equation can be obtained as follows [25].

$$\begin{bmatrix} x \\ y \end{bmatrix}_{k+1} = \Phi_k \begin{bmatrix} x \\ y \end{bmatrix}_k + W_k \quad (15)$$

where,

$$\Phi_k = e^{AT} = L^{-1}([sI - A]^{-1}) = \begin{bmatrix} 1 & 0 \\ 0 & 1 \end{bmatrix} \quad (16)$$

$$W_k = \int_{kT}^{(k+1)T} e^{A[(k+1)T-\tau]} \cdot B \cdot w(\tau) d\tau \quad (17)$$

The covariance matrix of state noise W_k can be expressed as

$$Q_w = E[W_k W_k^T] = \sigma_w^2 \begin{bmatrix} T & 0 \\ 0 & T \end{bmatrix} = \sigma_w^2 T \begin{bmatrix} 1 & 0 \\ 0 & 1 \end{bmatrix} \quad (18)$$

from (18), an important conclusion can be known that Q_w is related to sampling cycle T .

The state–space dimension of the distorted AC signal is extended under the consideration of fundamental and harmonic components. The state-space formulas of PAVD model

are the same as the conventional PAV model (2)–(3). The difference is that the state noise covariance in (4). The state noise covariance of the PAVD model is

$$Q_k = \sigma_{PAVD}^2 I_{2n \times 2n} = \rho T I_{2n \times 2n} \quad (19)$$

where, σ_{PAVD}^2 is the state noise covariance of PAVD model. $\rho \leq 1$ is a coefficient. When high detection precision is required, ρ is selected as a small value. When dynamic fast detecting is required, ρ is selected to a large value. Then, the discrete PAVD–KF algorithm can be obtained by combining model (2), (3), (15) and KF algorithm.

3.2. OVD–KF Algorithm

In the two-dimensional space, the circular movement of the object along the midpoint is projected on the x, y axis as a pure sine and a pure cosine waveform. It is shown in Figure 1.

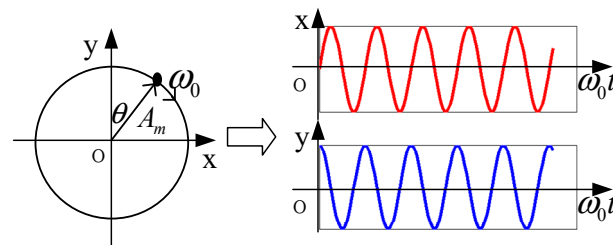


Figure 1. Diagram of the object circular movement being projected.

It can be expressed as

$$\begin{cases} x(t) = A_m \sin(\omega_0 t + \theta) \\ y(t) = A_m \cos(\omega_0 t + \theta) \end{cases} \quad (20)$$

where, A_m is the amplitude, ω_0 is the angular frequency, and θ is the phase angle.

The first derivative of (10) can be expressed as

$$\begin{cases} \dot{x}(t) = \omega_0 A_m \cos(\omega_0 t + \theta) + w_x(t) = \omega_0 y(t) + w_x(t) \\ \dot{y}(t) = -\omega_0 A_m \sin(\omega_0 t + \theta) + w_y(t) = -\omega_0 x(t) + w_y(t) \end{cases} \quad (21)$$

where, $w_x(t)$ and $w_y(t)$ are the input white noise, $w_x(t) \perp w_y(t)$. $w_x(t) \sim (0, \sigma_w^2)$, $w_y(t) \sim (0, \sigma_w^2)$.

The state equation can be obtained from (21).

$$\frac{d}{dt} \begin{bmatrix} x(t) \\ y(t) \end{bmatrix} = A \begin{bmatrix} x(t) \\ y(t) \end{bmatrix} + B \begin{bmatrix} w_x(t) \\ w_y(t) \end{bmatrix} = \begin{bmatrix} 0 & \omega_0 \\ -\omega_0 & 0 \end{bmatrix} \begin{bmatrix} x(t) \\ y(t) \end{bmatrix} + \begin{bmatrix} 1 & 0 \\ 0 & 1 \end{bmatrix} \begin{bmatrix} w_x(t) \\ w_y(t) \end{bmatrix} \quad (22)$$

Equation (22) is discretized, and the state equation can be obtained as follows [25].

$$\begin{bmatrix} x \\ y \end{bmatrix}_{k+1} = \Phi_k \begin{bmatrix} x \\ y \end{bmatrix}_k + W_k \quad (23)$$

where,

$$\Phi_k = e^{AT} = L^{-1}([sI - A]^{-1}) = \begin{bmatrix} \cos(\omega_0 T) & \sin(\omega_0 T) \\ -\sin(\omega_0 T) & \cos(\omega_0 T) \end{bmatrix} \quad (24)$$

$$W_k = \int_{kT}^{(k+1)T} e^{A[(k+1)T-\tau]} \cdot B \cdot w(\tau) d\tau \quad (25)$$

The state noise covariance matrix can be expressed as

$$Q_w = E[W_k W_k^T] = \sigma_w^2 \begin{bmatrix} T & 0 \\ 0 & T \end{bmatrix} = \sigma_w^2 T \begin{bmatrix} 1 & 0 \\ 0 & 1 \end{bmatrix} \quad (26)$$

from Equation (16), an important conclusion can be drawn that Q_w is related to the sampling cycle T .

The state-space dimension of the distorted AC signal is expanded under the consideration of fundamental and harmonic components. The state and measurement equations of OVD model are the same as the conventional OV model (4) and (5). The difference is that state noise covariance matrix of the OV model in (6). That is

$$Q_k = \sigma_{OVD}^2 I_{2n \times 2n} = \rho T I_{2n \times 2n} \quad (27)$$

where σ_{OVD}^2 is the covariance of OVD model. $\rho \leq 1$ is a coefficient. When high detection precision is required, ρ is selected as a small value. When dynamic fast detecting is required, ρ is selected to a large value.

Then, there are the combinations of the model (7), (8), (27), and KF algorithm. The discrete OVD–KF algorithm can be obtained.

4. Experiment and Evaluation

In this section, we conduct the detection of the current and the voltage with the sampling cycle of 10 μ s and 40 μ s. Then, comparing the detecting results for fundamental and harmonics components in PAVD–KF and PAV–KF algorithm, and in OVD–KF and OV–KF algorithm. At the last, we come to a conclusion of these results.

4.1. Experiment and Evaluation for AC Current Detection

4.1.1. Experiment Settings

As an experimental example, we sample the AC distorted current signal. Experiment platform consists of AC grid (380 V, 50 Hz), oscilloscope (Tektronix GDS–2102) and nonlinear load (the three–phase rectifier, $R = 100 \Omega$ and $L = 1.5 \text{ mH}$). It is shown in Figure 2. The AC current signals are sampled by the oscilloscope. Sampling cycles are selected as 10 μ s and 40 μ s. The experiment sampling current data and spectrogram are shown in Figures 3 and 4. The HRI of harmonic components are measured to be approximately 24% of 5th, 10% of 7th, 10% of 11th, 5% of 13th, 5% of 17th, 4% of 19th by spectrum analysis.

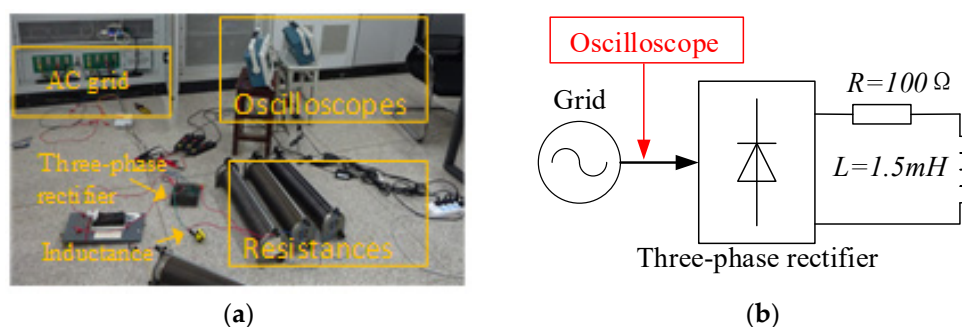


Figure 2. Experiment platform. (a) Current sampling experiment platform (b) Principle diagram of experiment platform.

HRI is defined as follows

$$\text{HRI}_n = \frac{I_n}{I_1} \times 100\% \quad (28)$$

where I_1 is the voltage rms value of fundamental component, I_n is the voltage rms value of n –th harmonic components.

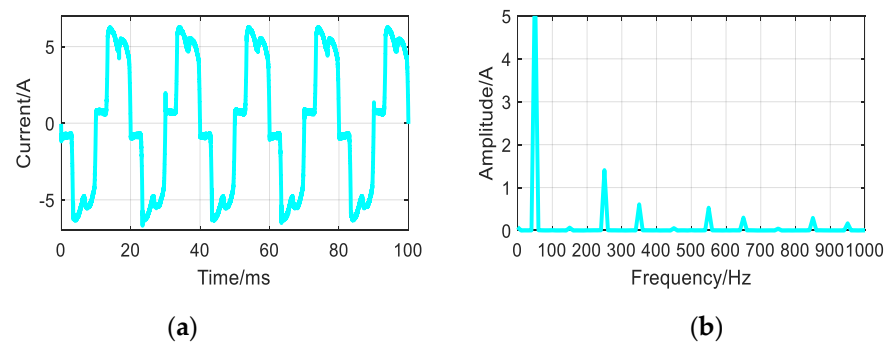


Figure 3. Experiment current for sampling cycle 10 μ s. (a) The sampling current data. (b) Spectrogram of sampling current data.

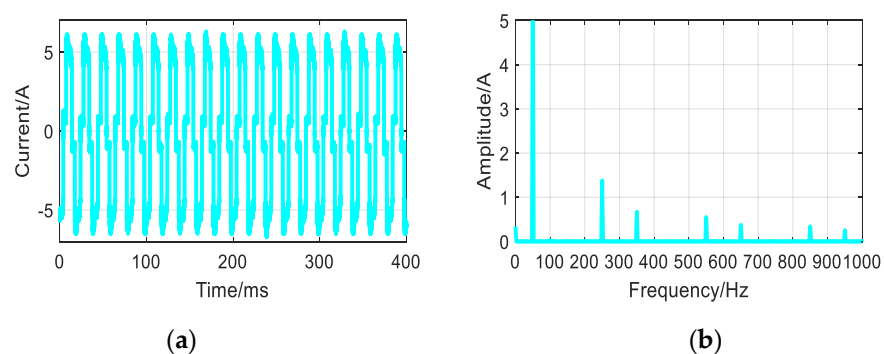


Figure 4. Experiment current for sampling cycle 40 μ s. (a) The sampling current data. (b) Spectrogram of sampling current data.

The measurement noise covariance R of the algorithms is all selected as 0.06 A, that is the measurement error of the sensor. The initial covariance matrices are selected as $P_{0/0} = 1000 \times I_{14 \times 14}$. The state noise covariance is selected as $Q_k = 0.01 \times I_{14 \times 14}$ in (4). The state noise covariance is selected as $Q_k = 0.01 \times T \times I_{14 \times 14}$ in (19).

4.1.2. Detection Results for PAVD–KF Algorithm

Two algorithms of PAV–KF and PAVD–KF are evaluated and compared. The evaluation results for sampling cycle 10 μ s and 40 μ s are shown in Figures 5 and 6.

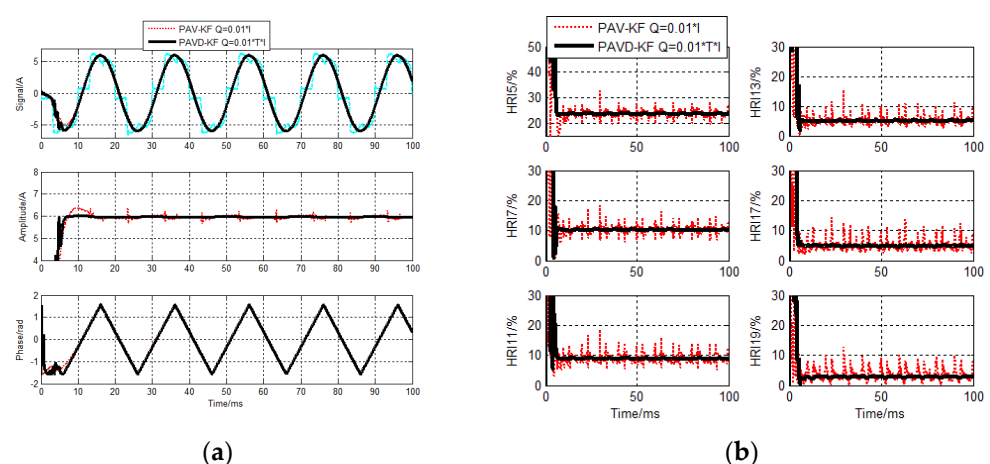


Figure 5. PAVD–KF current detecting results for sampling cycle 10 μ s. (a) Fundamental components detecting results (b) HRI detecting results.

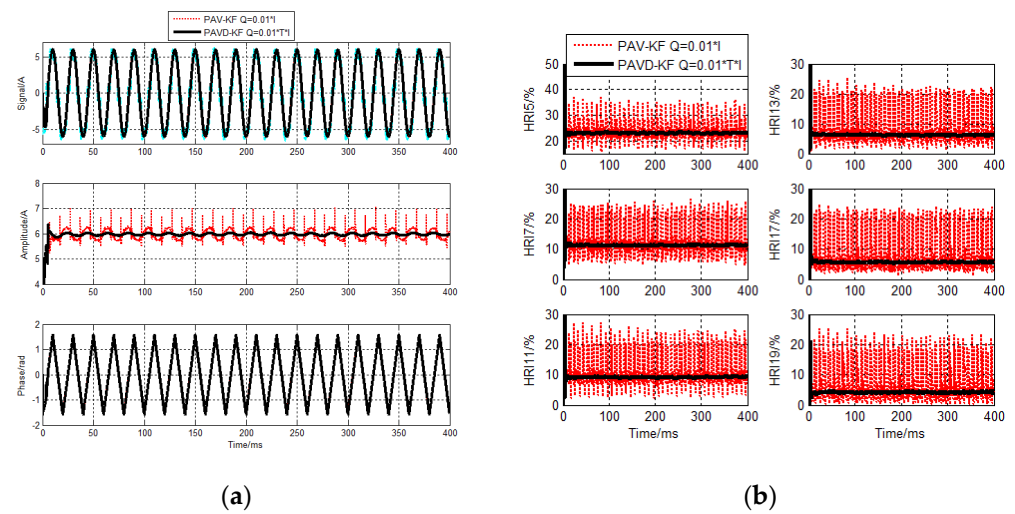


Figure 6. PAVD–KF current detecting results for sampling cycle $40 \mu s$. (a) Fundamental components detecting results (b) HRI detecting results.

4.1.3. Detection Results for OVD–KF Algorithm

Two algorithms of OV–KF and OVD–KF are evaluated and compared. The evaluation results for sampling cycle $10 \mu s$ and $40 \mu s$ are shown in Figures 7 and 8.

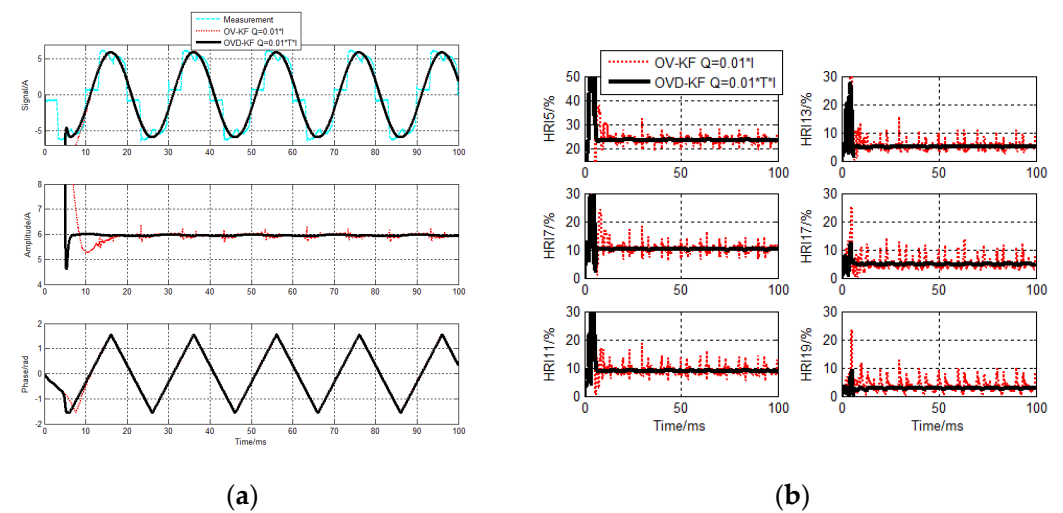


Figure 7. OVD–KF current detecting results for sampling cycle $10 \mu s$. (a) Fundamental components detecting results (b) HRI detecting results.

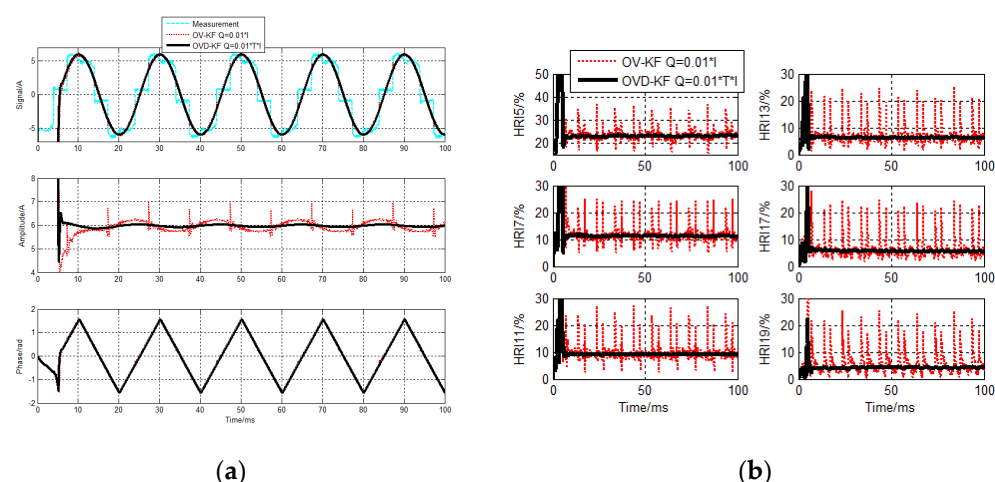


Figure 8. OVD–KF current detecting results for sampling cycle 40 μ s. (a) Fundamental components detecting results (b) HRI detecting results.

4.1.4. Summary for AC Current Detecting

It can be seen from Figures 5 and 8, when $Q = 0.01 \times I$, the detecting errors of the conventional PAV–KF and OV–KF algorithms are big. In particular, the detecting errors of the conventional algorithms for sampling cycle 40 μ s are rather big. The errors are too big to affect the normal operation.

Corresponding to it, when Q combines with the sampling cycle, $Q = 0.01 \times T \times I$, regardless of the fundamental or harmonic components, the proposed detecting accuracies in PAVD–KF and OVD–KF algorithm are much higher than the conventional algorithms.

4.2. Experiment and Evaluation for AC Voltage Detection

4.2.1. Experiment Settings

The AC signal is grid voltage as an experimental example. Experiment platform is shown in Figure 9. The experiment of superimposing harmonics in fundamental voltage is carried out through a programmable power supply device. The AC voltage signals are sampled and the sampling cycles T are selected by the oscilloscope of Tektronix GDS–2102.

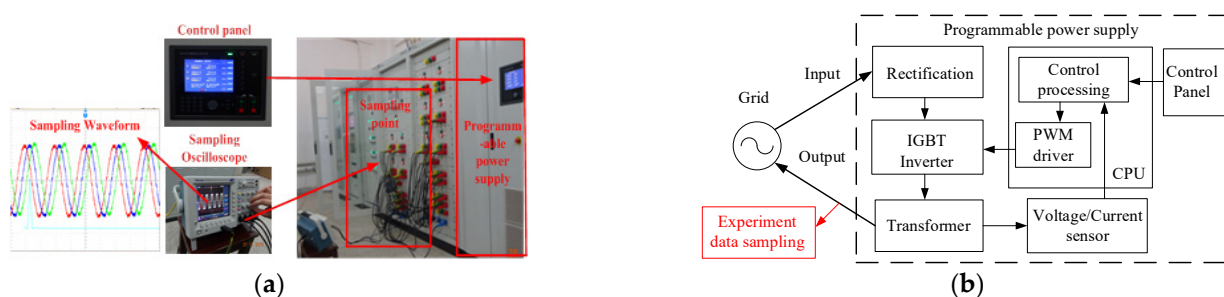


Figure 9. Experiment platform. (a) Voltage sampling experiment platform. (b) Principle diagram of experiment platform.

The harmonics ratio for voltage (HRU) is defined as follows

$$\text{HRU}_n = \frac{U_n}{U_1} \times 100\% \quad (29)$$

where U_1 is the voltage rms value of the fundamental component, and U_n is the voltage rms value of n –th harmonic components.

Experiment voltage data for sampling cycle 10 μ s is in Figure 10. Experiment voltage data for sampling cycle 40 μ s is in Figure 11, and the HRU of harmonic components all are set as 5% of 3rd, 10% of 5th, and 8% of 7th.

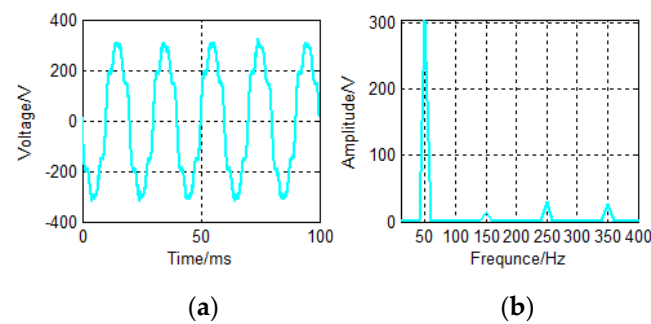


Figure 10. Experiment voltage for sampling cycle 10 μ s. (a) The sampling voltage data. (b) Spectrogram of sampling voltage data.

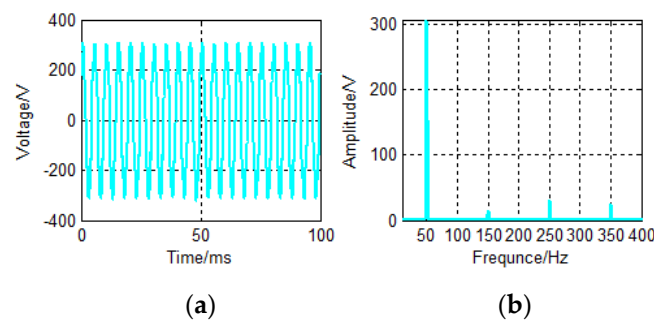


Figure 11. Experiment voltage for sampling cycle 40 μ s. (a) The sampling voltage data. (b) Spectrogram of sampling voltage data.

The R of the algorithms are all selected as 3.11 V, that is the measurement error of the sensor. The initial covariance matrices of algorithms are selected as $P_{0/0} = 1000 \times I_{10 \times 10}$. The state noise covariance matrix of algorithms is selected as $Q_k = 0.05 \times I_{10 \times 10}$. The state noise covariance matrix of algorithms is $Q_k = 0.1 \times T \times I_{10 \times 10}$.

4.2.2. Detection Results for PAVD–KF Algorithm

PAVD–KF and PAV–KF algorithms are evaluated and compared. The detecting results of the sampling cycle 10 μ s and 40 μ s are shown in Figures 12 and 13.

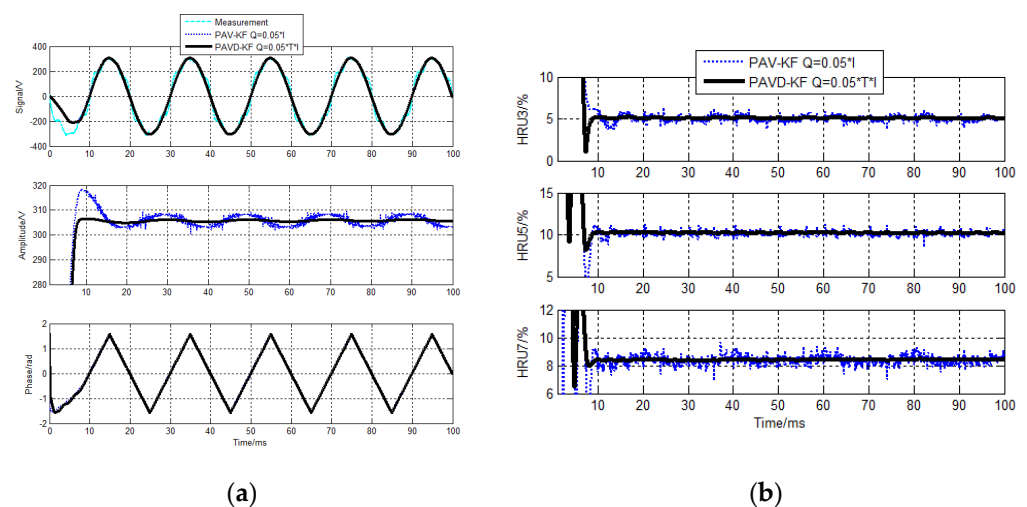


Figure 12. PAVD–KF voltage detecting results for sampling cycle 10 μ s. (a) Fundamental components detecting results (b) HRU detecting results.

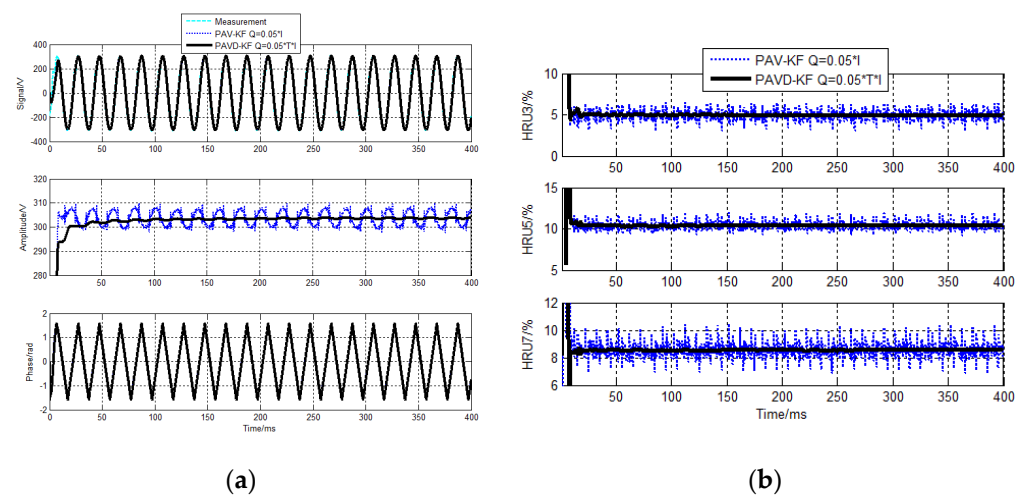


Figure 13. PAVD–KF voltage detecting results for sampling cycle 40 μs. (a) Fundamental components detecting results (b) HRU detecting results.

4.2.3. Detection Results for OVD–KF Algorithm

OVD–KF and OV–KF algorithms are evaluated and compared. The detecting results of the sampling cycle 10 μs and 40 μs are shown in Figures 14 and 15.

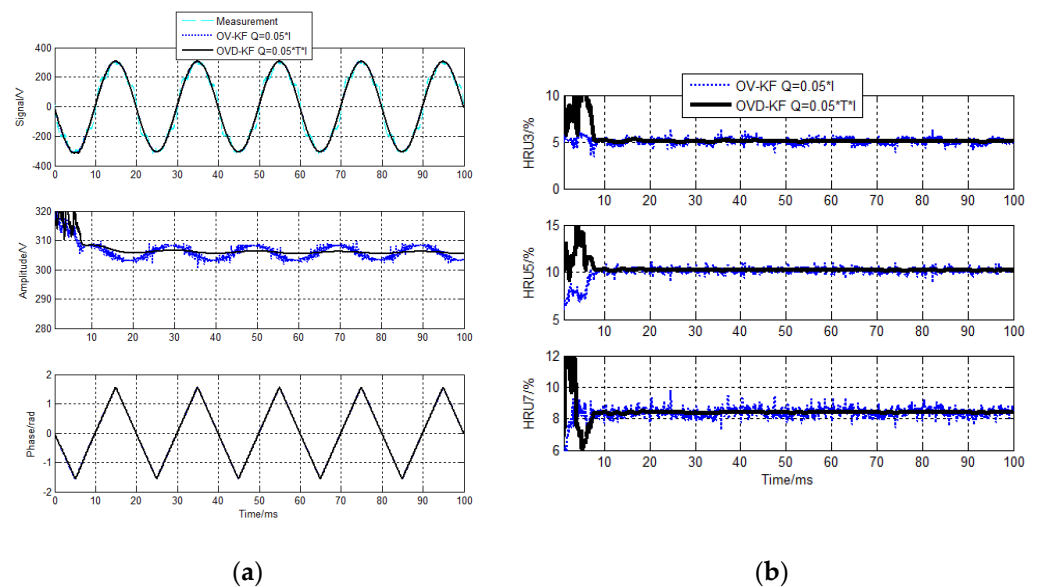


Figure 14. OVD–KF voltage detecting results for sampling cycle 10 μs. (a) Fundamental components detecting results (b) HRU detecting results.

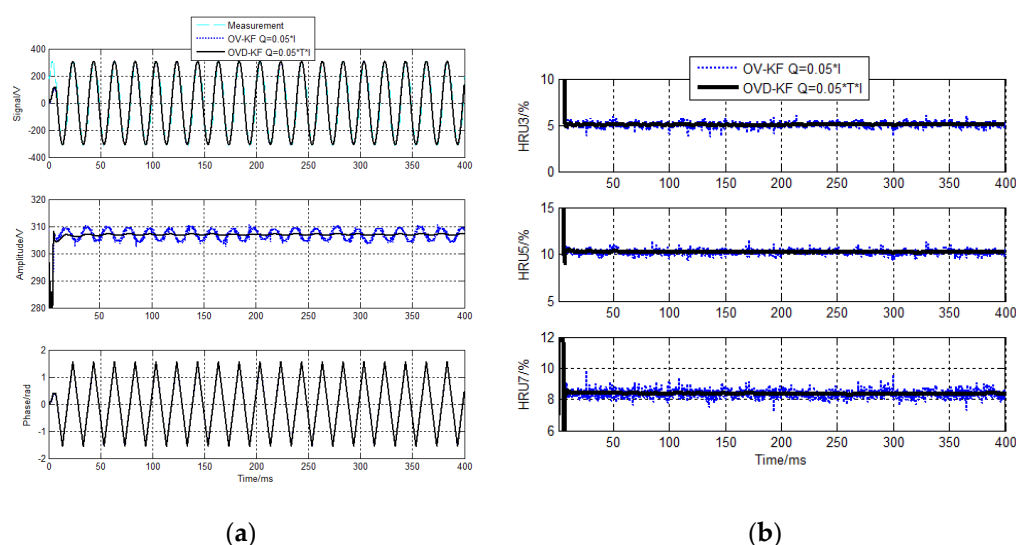


Figure 15. OVD–KF voltage detecting results for sampling cycle $40\ \mu\text{s}$. (a) Fundamental components detecting results (b) HRU detecting results.

4.2.4. Summary for AC Voltage Detecting

It can be seen from Figures 12 and 13 that the amplitudes of the fundamental components of the conventional model–KF algorithm detecting are fluctuating, the stability of its detection shows poorly. Specifically, when we use the sampling cycle $40\ \mu\text{s}$, the error is too big to be ignored. From Figures 14 and 15, we know that detecting errors of the harmonics components for the conventional OV–KF algorithm are also big, though the error seems smaller compared to PAV–KF. Corresponding to it, the detecting accuracies of the fundamental and harmonic components for the OVD–KF algorithm are higher than that of the OV–KF algorithm.

Generally, when $Q = 0.05 \times I$, the conventional algorithms could basically meet the engineering requirements with some big errors under different sampling cycle conditions. When $Q = 0.05 \times T \times I$, all the novel algorithms could fulfill the requirements.

4.3. Summary for Experiment and Evaluation

In general, when using the fixed value, the error of PAV model is the biggest, neither current nor voltage can meet the demand. OV model performs better, when using the sampling cycle $10\ \mu\text{s}$, the voltage can be used normally, and the current error is too big to be used. But when using the sampling cycle $40\ \mu\text{s}$, both current and voltage cannot operate normally.

The proposed algorithms in this paper, whether it is PAVD model or OVD model, it is related to the sampling cycle, so the voltage and current detecting results can meet the engineering requirement.

Take PAV model with $40\ \mu\text{s}$ in current and voltage tracking for example, the conventional methods produce big errors when $Q = 0.01 \times I$ detecting the current and $Q = 0.05 \times I$ detecting the voltage. Only when $Q = 0.00001 \times I$ detecting the current, the accuracy of it would be almost close to that of our proposed algorithm, as Figure 16 shows. When $Q = 0.0005 \times I$ detecting the voltage, the accuracy would satisfy the requirement, as Figure 17 shows.

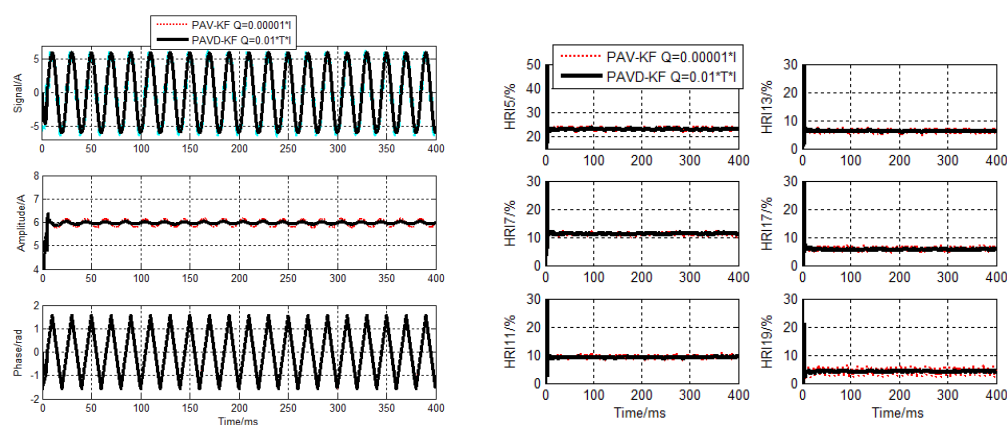


Figure 16. PAVD–KF current detecting results for sampling cycle 40 μ s. ($Q = 0.00001 \times I$).

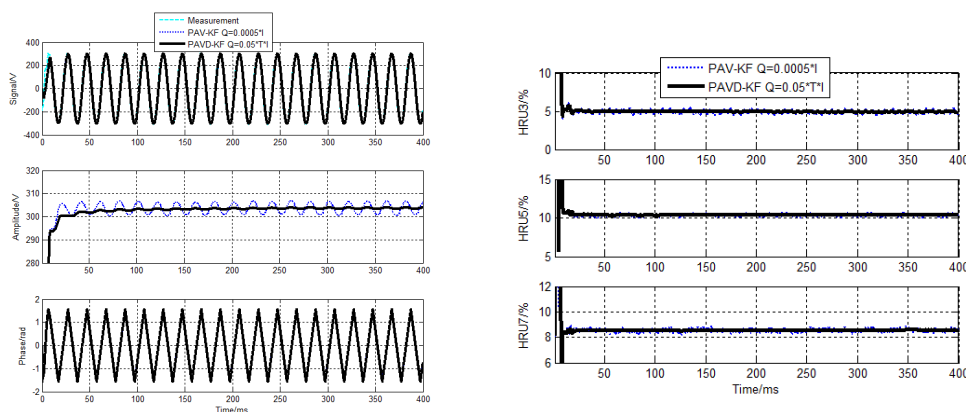


Figure 17. PAVD–KF voltage detecting results for sampling cycle 40 μ s. ($Q = 0.0005 \times I$).

5. Conclusions

This paper presents the PAVD–KF and OVD–KF algorithm derived from the stochastic process theory. It enhances the knowledge about the Kalman algorithms applied to the harmonic detection of the distorted AC grid. It gives a rule that the KF algorithms in the application of distorted grid AC signal detection is related to the sampling cycle and their state noise covariance cannot be simply considered as a constant.

This paper applies the actual current and voltage data of the sampling cycle 10 μ s and 40 μ s to detection and evaluation. The conventional algorithms have big errors in general and unable to meet engineering requirements. When using a fixed value of covariance, if we are going to obtain the ideal results, we need to spend a lot of time debugging (trying to make up) the parameters. Also, there is no theoretical source to set the fixed value of covariance. To solve it, we propose the algorithms to save much time and workload to get the ideal results. Besides, we make the algorithms more feasible and effective based on stochastic process theory. From which the results show that the proposed PAVD–KF and OVD–KF algorithms are effective and improve the dynamic detecting accuracy of grid AC signal significantly. This paper would provide a reference for the application of KF algorithms to harmonic detection, power quality control and grid synchronization in the future.

Author Contributions: Conceptualization, H.N. and X.N.; methodology, H.N. and X.N.; software, H.N.; validation, H.N. and X.N.; formal analysis, H.N.; investigation, H.N.; resources, H.N.; data curation, H.N.; writing—original draft preparation, H.N.; writing—review and editing, H.N.; visualization, H.N.; supervision, X.N.; project administration, X.N.; funding acquisition, X.N. All authors have read and agreed to the published version of the manuscript.

Funding: This research was funded by National Natural Science Foundations of China, grant number 51867017 “Research on Power Quality Dynamic Tracking and Real-time Detection Method for Micro-grid Complex Source Load Environment”.

Institutional Review Board Statement: Not applicable.

Informed Consent Statement: Not applicable.

Data Availability Statement: Not applicable.

Conflicts of Interest: The authors declare no conflict of interest.

References

- Auger, F.; Hilairat, M.; Guerrero, J.M.; Monmasson, E.; Orłowska-Kowalska, T.; Katsura, S. Industrial Applications of the Kalman Filter: A Review. *IEEE Trans. Ind. Electron.* **2013**, *60*, 5458–5471. [\[CrossRef\]](#)
- Girgis, A.A.; Brown, R.G. Application of Kalman Filtering In Computer Relaying. *IEEE Trans. Power Appar. Syst.* **1981**, *7*, 3387–3397. [\[CrossRef\]](#)
- Girgis, A.A.; Hwang, T.L.D. Optimal Estimation of Voltage Phasors and Frequency Deviation. *IEEE Trans. Power Appar. Syst.* **1984**, *10*, 2943–2951. [\[CrossRef\]](#)
- Girgis, A.A.; Sallam, A.A.; El-Din, A.K. Identification and tracking of harmonic sources in a power system using a Kalman filter. *IEEE Trans. Power Deliv.* **1998**, *13*, 414–420. [\[CrossRef\]](#)
- Nie, X. Detection of Grid Voltage Fundamental and Harmonic Components Using Kalman Filter Based on Dynamic Tracking Model. *IEEE Trans. Ind. Electron.* **2020**, *67*, 1191–1200. [\[CrossRef\]](#)
- Naseri, F.; Kazemi, Z.; Farjah, E.; Ghanbari, T. Fast Detection and Compensation of Current Transformer Saturation Using Extended Kalman Filter. *IEEE Trans. Power Deliv.* **2020**, *34*, 1087–1097. [\[CrossRef\]](#)
- Swain, S.; Subudhi, B. Grid Synchronization of a PV System with Power Quality Disturbances Using Unscented Kalman Filtering. *IEEE Trans. Sustain. Energy* **2019**, *10*, 1240–1247. [\[CrossRef\]](#)
- Uz-Logoglu, E.; Salor, O.; Ermis, M. Real-Time Detection of Interharmonics and Harmonics of AC Electric Arc Furnaces on GPU Framework. *IEEE Trans. Ind. Appl.* **2019**, *55*, 1373–1378.
- Xi, Y.; Tang, X.; Li, Z.; Cui, Y.; Zhao, T.; Zeng, X.; Guo, J.; Duan, W. Harmonic estimation in power systems using an optimised adaptive Kalman filter based on PSO-GA. *IET Gener. Transm. Distrib.* **2019**, *13*, 3968–3979. [\[CrossRef\]](#)
- Bagheri, A.; Mardaneh, M.; Rajaei, A.; Rahideh, A. Detection of Grid Voltage Fundamental and Harmonic Components Using Kalman Filter and Generalized Averaging Method. *IEEE Trans. Power Electron.* **2016**, *31*, 1064–1073. [\[CrossRef\]](#)
- Cardoso, R.; Camargo, R.F.; Pinheiro, H.; Grundling, H.A. Kalman filter based synchronisation methods. *IET Gener. Transm. Distrib.* **2008**, *2*, 542–555. [\[CrossRef\]](#)
- Swain, S.; Subudhi, B. Iterated extended Kalman filter-based grid synchronisation control of a PV system. *IET Energy Syst. Integr.* **2019**, *1*, 219–228. [\[CrossRef\]](#)
- Ferrero, R.; Pegoraro, P.A.; Toscani, S. Synchrophasor Estimation for Three-Phase Systems Based on Taylor Extended Kalman Filtering. *IEEE Trans. Instrum. Meas.* **2020**, *69*, 6723–6730. [\[CrossRef\]](#)
- Golestan, S.; Guerrero, J.M.; Vasquez, J.C.; Abusorrah, A.M.; Al-Turki, Y. Single-Phase FLLs Based on Linear Kalman Filter, Limit-Cycle Oscillator, and Complex Bandpass Filter: Analysis and Comparison With a Standard FLL in Grid Applications. *IEEE Trans. Power Electron.* **2019**, *34*, 1064–1073. [\[CrossRef\]](#)
- Ahmed, H.; Biricik, S.; Benbouzid, M. Linear Kalman Filter-Based Grid Synchronization Technique: An Alternative Implementation. *IEEE Trans. Ind. Inform.* **2021**, *17*, 3847–3856. [\[CrossRef\]](#)
- Alam, S.J.; Arya, S.R. Control of UPQC based on steady state linear Kalman filter for compensation of power quality problems. *Chin. J. Electr. Eng.* **2020**, *6*, 52–65. [\[CrossRef\]](#)
- Xi, Y.; Li, Z.; Zeng, X.; Tang, X.; Liu, Q.; Xiao, H. Detection of power quality disturbance using an adaptive process noise covariance Kalman filter. *Digit. Signal Process.* **2018**, *76*, 34–49. [\[CrossRef\]](#)
- Wu, C.; Magana, M.E.; Cotilla-Sanchez, E. Dynamic Frequency and Amplitude Estimation for Three-Phase Unbalanced Power Systems Using the Unscented Kalman Filter. *IEEE Trans. Instrum. Meas.* **2019**, *68*, 3387–3395. [\[CrossRef\]](#)
- Panigrahi, R.; Subudhi, B.; Panda, P.C. A robust LQG servo control strategy of shunt-active power filter for power quality enhancement. *IEEE Trans. Power Electron.* **2016**, *31*, 2860–2869. [\[CrossRef\]](#)
- Panigrahi, R.; Subudhi, B. Performance enhancement of shunt active power filter using a Kalman filter-based H_∞ control strategy. *IEEE Trans. Power Electron.* **2017**, *32*, 2622–2630. [\[CrossRef\]](#)
- Abdelsalam, A.A.; Abdelaziz, A.Y.; Kamh, M.Z. A Generalized Approach for Power Quality Disturbances Recognition Based on Kalman Filter. *IEEE Access* **2021**, *9*, 93614–93628. [\[CrossRef\]](#)
- Xi, Y.; Li, Z.; Tang, X.; Zeng, X. Classification of power quality disturbances based on KF-ML-Aided S-Transform and multilayers feedforward neural networks. *IET Gener. Trans. Distrib.* **2020**, *14*, 4010–4020. [\[CrossRef\]](#)
- Abdelsalam, A.A.; Eldesouky, A.A.; Sallam, A.A. Classification of Power System Disturbances using Linear Kalman Filter and Fuzzy-expert System. *Electr. Power Energy Syst.* **2012**, *43*, 688–695. [\[CrossRef\]](#)

-
24. Abdelsalam, A.A.; Eldesouky, A.A.; Sallam, A.A. Characterization of power quality disturbances using hybrid technique of linear Kalman filter and fuzzy-expert system. *Electr. Power Syst. Res.* **2012**, *83*, 41–50. [[CrossRef](#)]
 25. Brown, R.G.; Hwang, P.Y.C. *Introduction to Random Signals and Applied Kalman Filtering with MATLAB Exercises*, 4th ed.; John Wiley & Sons, Inc.: Hoboken, NJ, USA, 2011.